Physics in Medicine & Biology

IPEM Institute of Physics and Engineering in Medicine

CrossMark

PAPER

The first prospective implementation of markerless lung target tracking in an experimental quality assurance procedure on a standard linear accelerator

Marco Mueller[1,5] , Reza Zolfaghari[1], Adam Briggs[2], Hugo Furtado[4], Jeremy Booth[2], Paul Keall[1], Doan Nguyen[1,3] , Ricky O'Brien[1] and Chun-Chien Shieh[1]

[1] ACRF Image X Institute, The University of Sydney, Sydney, NSW, Australia
[2] Northern Sydney Cancer Centre, Royal North Shore Hospital, Sydney, NSW, Australia
[3] School of Biomedical Engineering, University of Technology Sydney, Sydney, NSW, Australia
[4] Department of Radiation Oncology & Christian Doppler Laboratory for Medical Radiation Research for Radiation Oncology, Medical University of Vienna, Vienna, Austria
[5] Author to whom any correspondence should be addressed.

E-mail: marco.mueller@sydney.edu.au

Abstract

The ability to track tumour motion without implanted markers on a standard linear accelerator (linac) could enable wide access to real-time adaptive radiotherapy for cancer patients. We previously have retrospectively validated a method for 3D markerless target tracking using intra-fractional kilovoltage (kV) projections acquired on a standard linac. This paper presents the first prospective implementation of markerless lung target tracking on a standard linac and its quality assurance (QA) procedure. The workflow and the algorithm developed to track the 3D target position during volumetric modulated arc therapy treatment delivery were optimised. The linac was operated in clinical QA mode, while kV projections were streamed to a dedicated computer using a frame-grabber software. The markerless target tracking accuracy and precision were measured in a lung phantom experiment under the following conditions: static localisation of seven distinct positions, dynamic localisation of five patient-measured motion traces, and dynamic localisation with treatment interruption. The QA guidelines were developed following the AAPM Task Group 147 report with the requirement that the tracking margin components, the margins required to account for tracking errors, did not exceed 5 mm in any direction. The mean tracking error ranged from 0.0 to 0.9 mm (left–right), −0.6 to −0.1 mm (superior–inferior) and −0.7 to 0.1 mm (anterior–posterior) over the three tests. Larger errors were found in cases with large left–right or anterior–posterior and small superior–inferior motion. The tracking margin components did not exceed 5 mm in any direction and ranged from 0.4 to 3.2 mm (left–right), 0.7 to 1.6 mm (superior–inferior) and 0.8 to 1.5 mm (anterior–posterior). This study presents the first prospective implementation of markerless lung target tracking on a standard linac and provides a QA procedure for its safe clinical implementation, potentially enabling real-time adaptive radiotherapy for a large population of lung cancer patients.

1. Introduction

Lung tumours have significant inter- and intrafraction motion, which introduces a major source of uncertainty for lung cancer radiotherapy during both treatment planning and delivery (Suh *et al* 2008). In the current standard of care, the movement of tumours is not tracked, and is accounted for by adding margins around the target volume (Brandner *et al* 2017), imposing additional dose to healthy tissues. Many techniques such as deep inspiration breath-hold (Hanley *et al* 1999), active breath-hold (Wong *et al* 1999) or abdominal compression (Heinzerling *et al* 2007) have been proposed to regulate the breathing and consequently target motion. However many lung cancer patients are not able to adopt these techniques as they suffer from breathing difficulties. The use

of advanced imaging systems such as ultra-sound (Hsu *et al* 2005, Maurer *et al* 2015), MRI (Glitzner *et al* 2019, Han and Zhou 2019) and dual energy kV imaging (Haytmyradov *et al* 2019) can enable intra-fractional target tracking, however these are less accessible and require additional costs compared with standard radiotherapy systems. Alternatively, radiation beam gating techniques (Takao *et al* 2016, Rouabhi *et al* 2018) prolong total treatment times while decreasing treatment efficacy and approaches utilising correlated surrogates such as surface guidance techniques (Hoisak and Pawlicki 2018) or diaphragm tracking (Cerviño *et al* 2009, Hindley *et al* 2019) do not track the target directly and can suffer under unforeseen motion patterns.

Target tracking is a challenging task when using the on-board kilovoltage (kV) imaging system (Yin *et al* 2009) on a standard linear accelerator (linac) due to two factors. First, the visibility of the target is often poor in the kV projection and can vary widely as the gantry rotates in a volumetric modulated arc therapy (VMAT) session (Teske *et al* 2015). Second, as the kV beam is perpendicular to the megavoltage (MV) beam, it is necessary to infer the 3D position of the target based on the 2D observation from the kV projection. One solution to overcome poor target visibility is to insert radio-opaque markers (Shimizu *et al* 2001, Huang *et al* 2015, Kim *et al* 2017) or electro-magnetic transponders around the target (Rau *et al* 2008, Shah *et al* 2013, Booth *et al* 2016, Schmitt *et al* 2017). However the insertion of a beacon or a marker requires an interventional procedure which is undesirable for many patients.

To enable markerless target tracking, systems such as the XSight (Fu *et al* 2007) used in Cyberknife (Adler *et al* 1997) or the carbon-ion pencil beam system (Mori *et al* 2016) use fixed dual source imaging. These systems are, however, very rare and expensive. Markerless lung target tracking approaches have been proposed in retrospective studies using MV imaging (Richter *et al* 2010, Rottmann *et al* 2013, Bryant *et al* 2014, Serpa *et al* 2014), kV imaging (Hugo *et al* 2010, Lewis *et al* 2010, Gendrin *et al* 2012, Yang *et al* 2012, van Sörnsen de Koste *et al* 2015, Hirai *et al* 2019), or both (Furtado *et al* 2013, Ren *et al* 2014, Zhang *et al* 2018). Although markerless position verification for lung tumours treated in breath-hold has been tested clinically (Hazelaar *et al* 2018), the task of continuous target tracking remains challenging especially in clinical scenarios. No prospective implementation of markerless target tracking on a standard linac has been reported.

We have previously developed a markerless target tracking algorithm that overcomes the above-mentioned challenges. The challenge of variable and inferior target visibility, which is caused by the overlap between the target and its surrounding anatomic structures, was overcome by utilising patient-specific modelling for anatomic suppression. The 3D position of the target was inferred from the 2D projection space using an extended Kalman filter (Shieh *et al* 2017). The computation time was found to be 1–6 s for each kV frame, which was insufficient for real-time tracking.

The purpose of this work was to report on the next necessary step towards markerless lung target tracking on standard linacs: the prospective clinical implementation and development of a feasible clinical workflow. We have overcome the computation challenges from the previous retrospective work (Shieh *et al* 2015, 2017) and implemented it on a standard linac in phantom experiments ready for clinical use. We further detail a quality assurance (QA) procedure for markerless target tracking following the AAPM task group (TG) 147 recommendations (Willoughby *et al* 2012), QA for the Calypso system (Santanam *et al* 2009), and QA for a marker-based tracking technology (Ng *et al* 2014).
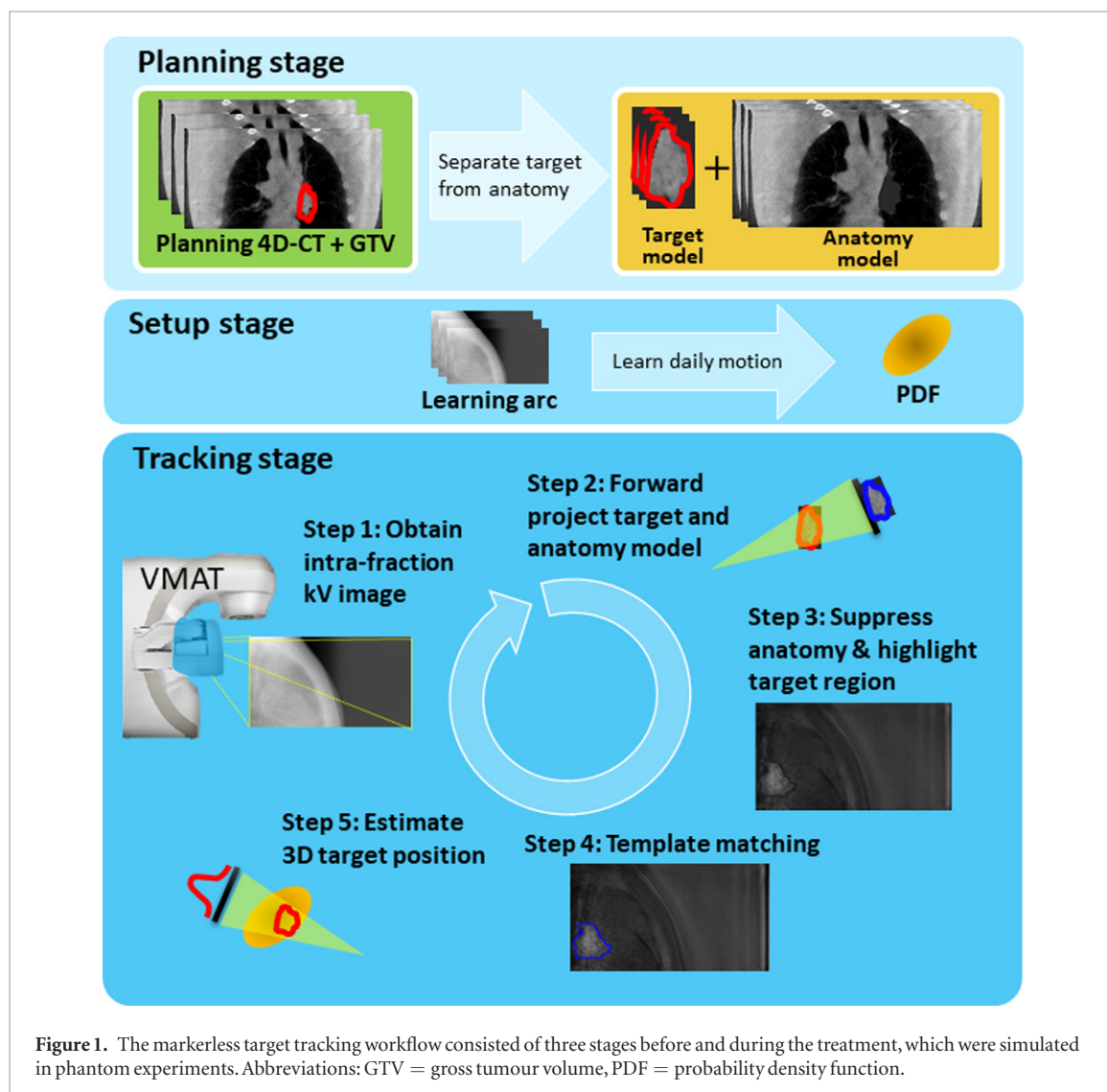
2. Methods

2.1. Markerless target tracking

Figure 1 provides an overview of our markerless target tracking method. More details and prove of feasibility can be found in the previous retrospective studies (Shieh *et al* 2015, 2017).

In the Planning stage, the planning 4D-CT and the gross tumour volume (GTV) contour were used to generate the target and anatomy models. The target model was the 4D-CT but with everything outside of the GTV contour masked out, whereas the anatomy model was the 4D-CT with voxels within the GTV contour removed. An initial target motion model was also built from the target position observed in each phase of the 4D-CT.

In the Setup stage, markerless target tracking was adapted to daily changes in the target motion pattern. On the day of the experiment and immediately prior to treatment delivery, a 200 degree kV projection arc was acquired over approximately 30 s. KV projections where the target was not obstructed by the spine were used for learning the motion pattern, which was then described in a motion model by a 3D Gaussian probability density function (PDF) (Poulsen *et al* 2008).

In the Tracking stage, the 3D position of the target was tracked on continuous kV projections in five steps during a VMAT treatment. For every new kV projection acquired (step 1), the anatomy model was forward-projected (step 2), and then rigidly aligned to and subtracted from the kV projection (step 3). This resulted in the 'anatomy-suppressed projection' with most of the contribution from overlapping anatomies removed and the target region highlighted. In step 4, the 2D coordinates of the target were located using template matching of the forward-projected target model in the 'anatomy-suppressed projection'. Finally, in step 5 the third dimen-

Figure 1. The markerless target tracking workflow consisted of three stages before and during the treatment, which were simulated in phantom experiments. Abbreviations: GTV = gross tumour volume, PDF = probability density function.

sion of the target position was inferred from the 2D coordinates using a Bayesian estimation framework (Shieh *et al* 2017).

2.2. Real-time implementation

Markerless target tracking was implemented in a VMAT treatment workflow following the clinical workflow for standard of care lung cancer radiotherapy. The linac was operated in clinical QA mode and kV projections were streamed directly from the linac to a dedicated computer (Lee *et al* 2018). To enable real-time computation of the 3D target position, the proposed algorithm was optimised in two aspects. First, the forward-projection calculation of both the anatomy and target models was implemented on a graphical processing unit (GPU) as described in Furtado *et al* (2013). With the GPU implementation, the computation time of the forward-projection step was reduced from a couple of seconds to below 100 ms. Second, the fast template matching module implemented in the OpenCV libraries (Bradski 2000) was used for aligning the forward-projected anatomy model and locating the 2D position of the target.

2.3. Experimental setup

Figure 2 shows the experimental setup on the linac. A CIRS lung phantom was used with a 2 cm spherical insert representing the target. To simulate 3D movement, the phantom was fixed on a modified HexaMotion platform where an in-house built board replaced the normal Delta4 device to enable the HexaMotion to move other phantoms.

2.3.1. Planning stage

4D-CT images were acquired on a Phillips Brilliance Big Bore CT with a pitch ratio of 0.05 at 120 kV/300 mA. The 4D-CT projection data were sorted into ten respiratory bins based on the external real-time position
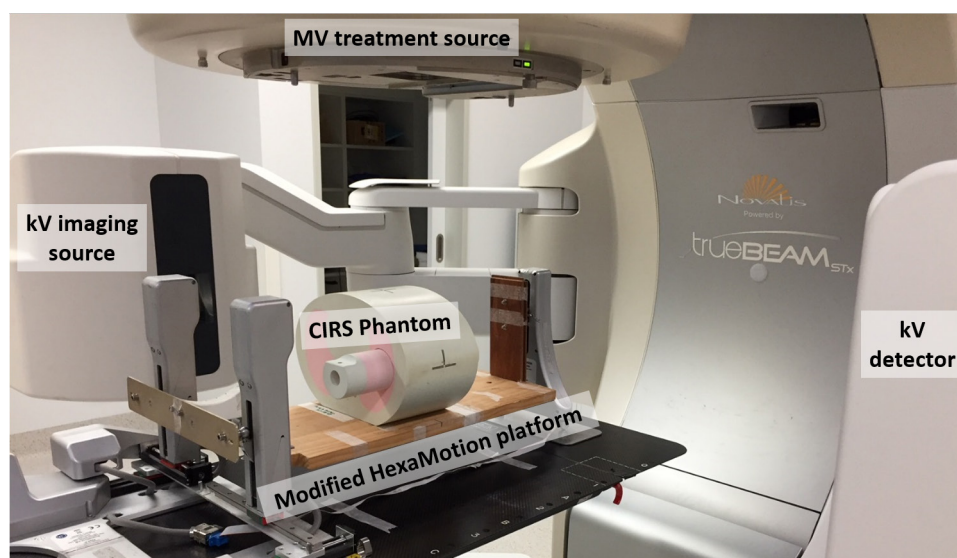
Figure 2. In the experimental setup the CIRS lung phantom was attached to a modified HexaMotion platform to emulate static and 3D motion traces that encompass different types of lung tumour motion during VMAT treatment on the linac.

management device signal and reconstructed with a resolution of $1.27 \times 2 \times 1.27$ mm^3. Subsequently, the target within the phantom was contoured and a VMAT plan (10 MV, 12 Gy/fx, ITV: D100% = 100% (12 Gy), PTV D98% >=100% (12 Gy), 2400 MU min^{-1}, flattening filter free) originated in RTOG0915 (Videtic *et al* 2015) was generated by a registered radiation therapist using the Eclipse planning system (Version 15.6). Finally, the anatomy and target models were built using the 4D-CT and GTV contours.

2.3.2. Setup and tracking stage

The phantom experiments were conducted on a Varian Truebeam (Version 2.7 MR2). At the beginning of the treatment session a half-fan cone-beam CT was obtained to align the phantom. For each experiment a pre-treatment learning arc was performed prior to starting the VMAT treatment. The pre-treatment arc consisted of 200 full-fan kV projections acquired over 200 degrees with an imaging rate of 7 Hz. Once the motion model was updated, the VMAT treatment was delivered with simultaneous kV acquisition.

The intrafraction kV projections were acquired at 7 Hz with a field size of 80×80 mm^2 at 80 kV/5 mA in between $-90°$ to $90°$ around the superior inferior axis. The source to detector distance was set to 150 cm in full-fan mode.

2.4. Quality assurance tests for markerless target tracking

The QA procedure for markerless target tracking was adopted from AAPM TG 147 (Willoughby *et al* 2012) and closely resembled the QA procedure for the Calypso system (Santanam *et al* 2009) and a marker-based technology (Ng *et al* 2014). We evaluated the markerless target tracking under three operational conditions: (1) static localisation, (2) dynamic localisation, and (3) dynamic localisation with treatment interruption. An end-to-end latency measurement was also performed.

The ground truth for the tracking performance validation was the HexaMotion target motion trace (input), which was synchronised with the tracked target motion (output) by maximising correlation. An analysis of the induced error due to this method resulted in an estimated error of <0.2 mm which is well below the total tracking accuracy error. Therefore, the induced error of this method was negligible. The tracking accuracy (mean tracking error in each dimension) and precision (standard deviation of tracking error in each dimension) were measured with respect to the ground truth.
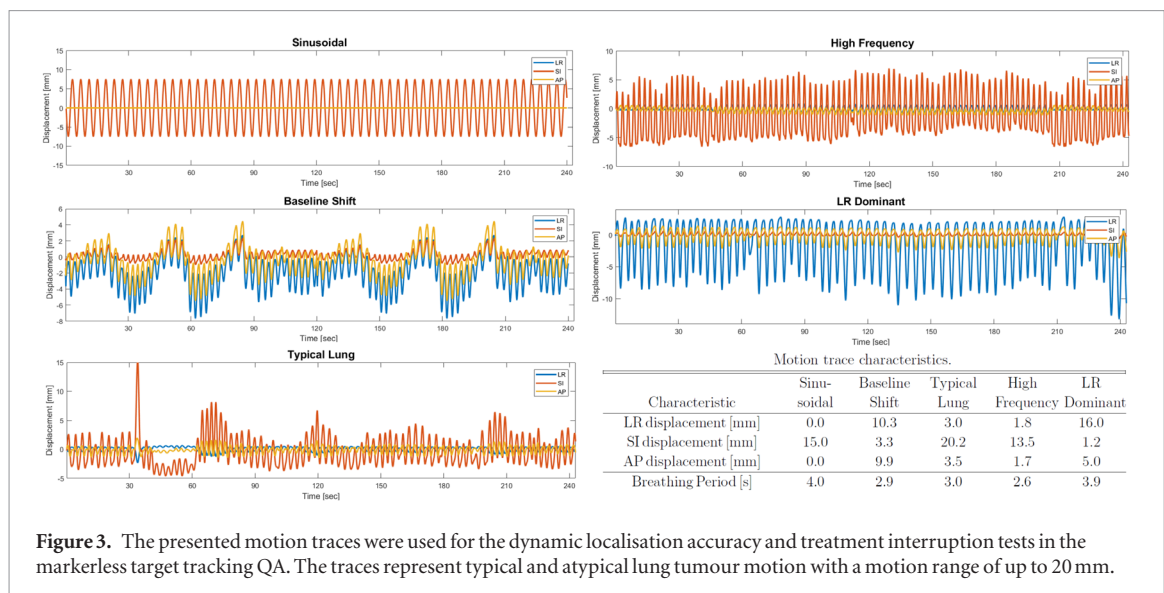
2.4.1. Static localisation accuracy

The static localisation accuracy tests evaluated the accuracy and precision of markerless target tracking over realistic clinical shifts of the target. For this purpose the CIRS phantom and the HexaMotion device were set up without any programmed motion. The target was aligned with the iso-centre and ±5 mm along each of the left right (LR), superior inferior (SI) and anterior posterior (AP) directions amounting to seven distinct positions.

2.4.2. Dynamic localisation accuracy

The dynamic localisation accuracy tests investigated the accuracy and precision of the markerless target tracking application for five motion traces as shown in figure 3. The ground truth was the synchronised HexaMotion trace.

Figure 3. The presented motion traces were used for the dynamic localisation accuracy and treatment interruption tests in the markerless target tracking QA. The traces represent typical and atypical lung tumour motion with a motion range of up to 20 mm.

Five different lung tumour motion traces used in a previously published study (Colvill *et al* 2016) were used: sinusoidal, baseline shift, typical lung, high frequency and LR dominant. Apart from the Sinusoidal trace, all the traces were originally acquired on a Cyberknife Synchrony machine from lung cancer patients at a sampling rate of 25 Hz and smoothed for practical use (Suh *et al* 2008). The traces were originally selected to represent a range of typical and atypical lung tumour motions. The movement was initiated at the beginning of the pre-treatment arc, which merged into the target tracking while the phantom continued moving with the same motion trace.

2.4.3. Dynamic localisation with treatment interruption

The treatment interruption tests examined how the algorithm performed when the treatment resumed after an interruption. After the first 10–20 s, the treatment beam and the kV imaging beam were manually paused , while the target motion continued. A couch shift was applied to align the drifted mean target location of the last 15 s to the iso-centre. Next the target tracking and the MV treatment were resumed. This test was to evaluate whether the suggested drift was correct and whether markerless target tracking proceeded successfully.

2.5. Latency measurement

For the end-to-end latency measurement, videos with 30 frames per second were used to capture both the markerless target tracking output and the phantom motion (from the camera in the treatment room) in an independent measurement. Next, seven motion peaks from both signals were matched and their time stamps in the camera images were compared. The mean and standard deviation of time difference was considered as the end-to-end latency. Additionally, the computation time for each incoming kV projection was recorded.

2.6. Quality assurance pass criteria

The QA requirement for the localisation tests was that the margins required to account for the tracking errors (tracking margin components) did not exceed 5 mm in any direction. This choice was motivated by the recommendations for lung stereotactic body radiotherapy (Videtic *et al* 2015). The tracking accuracy and precision were measured for the tracked target motion with respect to the synchronised HexaMotion trace. Finally, the tracking margin components were calculated according to Van Herk (2004) based on the average measured tracking accuracy and precision in each direction in each of the three localisation tests. Tracking is one margin component, and when combined with other errors it is designed to achieve a minimum dose to the clinical target volume of 95% for 90% of patients. In this study the margin component was composed of tracking accuracy and precision as defined as:

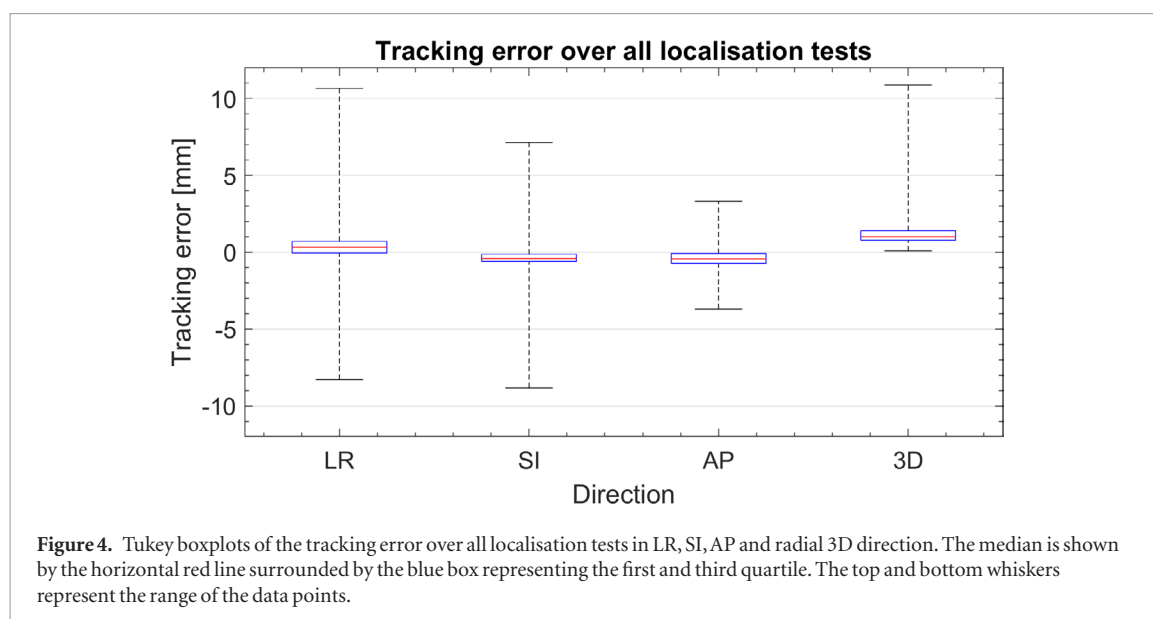$$Tracking\ Margin\ Component_{(LR,\,SI,\,AP)} = 2.5 \cdot Accuracy + 0.7 \cdot Precision$$

in each direction LR, SI and AP.

3. Results

3.1. Overall localisation accuracy

Figure 4 shows the Tukey boxplots of the tracking error summarised over all localisation tests. The mean $\pm$ standard deviation of the tracking error in each direction over all measurements was 0.5 ± 1.2 mm (LR), $-0.3 \pm$

Figure 4. Tukey boxplots of the tracking error over all localisation tests in LR, SI, AP and radial 3D direction. The median is shown by the horizontal red line surrounded by the blue box representing the first and third quartile. The top and bottom whiskers represent the range of the data points.

0.6 mm (SI) and -0.3 ± 0.8 mm (AP). The 3D tracking error (Euclidean norm over the three motion directions) was 1.3 ± 1.0 mm.

3.2. Static localisation accuracy

Figure 5(a) shows a plot of the localisation result using markerless target tracking for the target located at origin. Table 1 shows the static localisation test results. The mean $\pm$ standard deviation of the tracking error in each direction over all measurements was 0.0 ± 0.5 mm (LR), -0.6 ± 0.2 mm (SI) and -0.5 ± 0.4 mm (AP). These values led to tracking margin components of 0.4 mm (LR), 1.6 mm (SI) and 1.5 mm (AP). All static localisation measurements met the QA requirement.

3.3. Dynamic localisation accuracy

Figures 5(b) and (c) show the plots of the best (typical lung) and the worst (LR dominant) case of dynamic localisation measurements using markerless target tracking. For each motion trace, the measured target motion trace was compared to the synchronised HexaMotion trace. Table 2 summarises the dynamic localisation test results. The mean $\pm$ standard deviation of the tracking error in each direction over all measurements was 0.7 ± 1.4 mm (LR), -0.2 ± 0.5 mm (SI) and -0.7 ± 0.7 mm (AP). These values resulted in tracking margin components of 2.7 mm (LR), 0.9 mm (SI) and 2.2 mm (AP). All dynamic localisation measurements met the QA requirement.
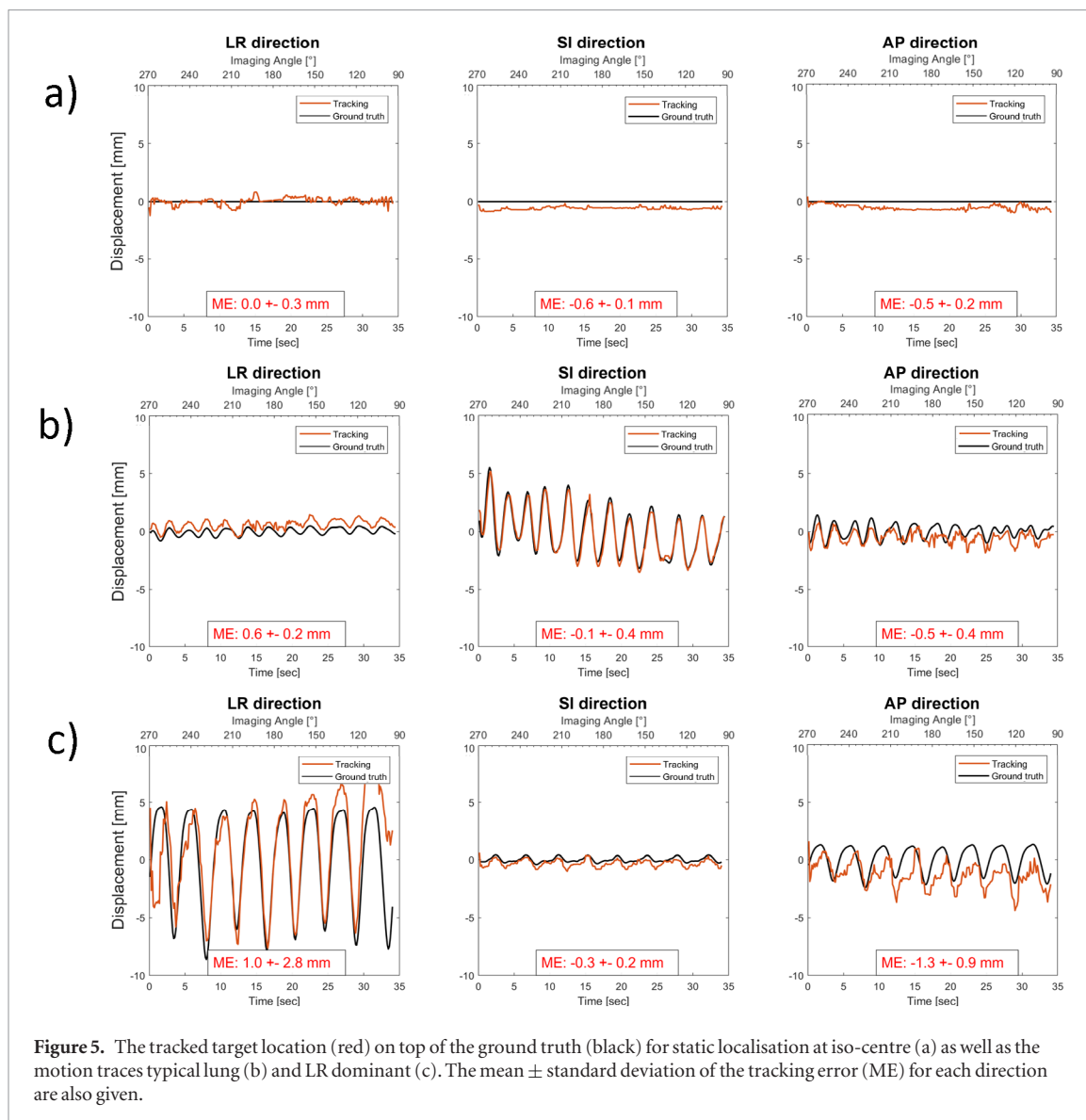
As the SI motion was always perpendicular to the imaging direction, we expected the SI errors to be low. Errors in the AP and LR directions were larger as they were not unambiguously resolved at every angle. The mean and standard deviation of the error in each direction was found to be <1 mm except for the baseline shift and LR dominant cases.

3.4. Dynamic localisation accuracy with treatment interruption

Figure 6 shows an example of a large baseline-shift in LR direction of the LR Dominant case. Table 3 shows the treatment interruption test results. The mean $\pm$ standard deviation of the tracking error in each direction over all measurements was 0.9 ± 1.3 mm (LR), -0.1 ± 0.6 mm (SI) and 0.1 ± 0.8 mm (AP). These values resulted in a tracking margin components of 3.2 mm (LR), 0.7 mm (SI) and 0.8 mm (AP). Similarly to the dynamic localisation accuracy test, sub-millimetre accuracy and precision were found except for the baseline shift and LR dominant cases. All treatment interruption tests met the QA requirement. Markerless target tracking successfully monitored the motion baseline shift and displayed the correct couch correction parameters when the treatment was interrupted.

3.5. Latency measurement

The mean $\pm$ standard deviation of the end-to-end latency was measured to 230 ± 17 ms. The mean $\pm$ standard deviation of the computation latency to process a kV projection was 94 ± 24 ms. The difference between computation and end-to-end latency, 136 ms, was the time to acquire, read and transfer the x-ray projection from the linac system to the dedicated computer.
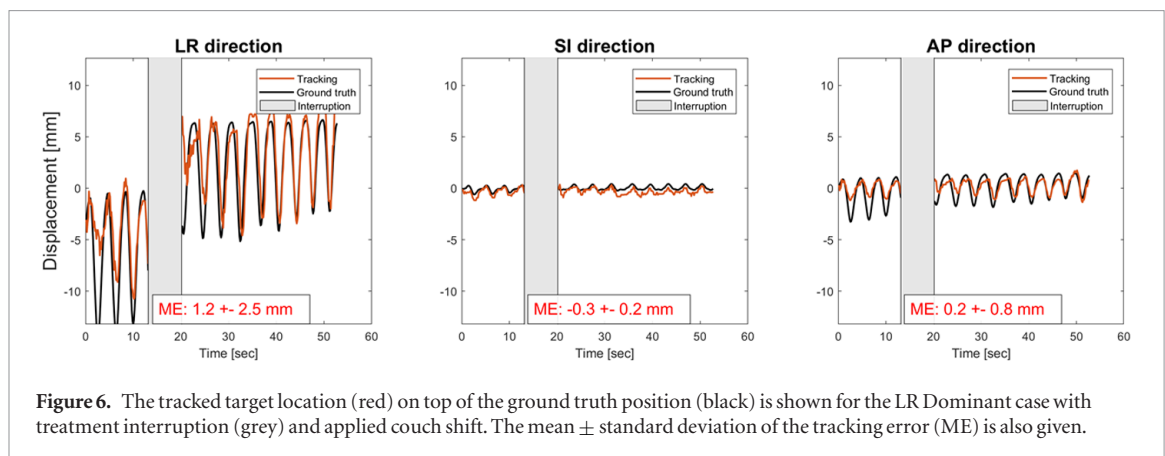
Figure 5. The tracked target location (red) on top of the ground truth (black) for static localisation at iso-centre (a) as well as the motion traces typical lung (b) and LR dominant (c). The mean ± standard deviation of the tracking error (ME) for each direction are also given.

Table 1. The static localisation test results are presented as the mean ± standard deviation of the tracking error in each of the three motion directions.

	Tracking error (mm)		
Target shift	LR	SI	AP
None	0.0 ± 0.3	-0.6 ± 0.1	-0.5 ± 0.2
5 mm left	-0.1 ± 0.5	-0.5 ± 0.1	-0.2 ± 0.2
5 mm right	0.1 ± 0.3	-0.7 ± 0.1	-0.7 ± 0.4
5 mm superior	-0.4 ± 0.7	-0.3 ± 0.2	-0.2 ± 0.3
5 mm inferior	0.1 ± 0.5	-0.7 ± 0.1	-0.7 ± 0.3
5 mm anterior	0.0 ± 0.3	-0.6 ± 0.1	-0.5 ± 0.2
5 mm posterior	0.1 ± 0.4	-0.6 ± 0.1	-0.6 ± 0.5

Table 2. The mean ± standard deviation of the tracking error in the dynamic localisation test.

	Tracking error (mm)		
Motion trace	LR	SI	AP
Sinusoidal	0.3 ± 0.9	-0.4 ± 0.8	-0.8 ± 0.4
Baseline shift	1.1 ± 1.3	-0.3 ± 0.2	-0.5 ± 0.8
Typical lung	0.6 ± 0.2	-0.1 ± 0.4	-0.5 ± 0.4
High frequency	0.7 ± 0.4	0.0 ± 0.8	-0.3 ± 0.6
LR dominant	1.0 ± 2.8	-0.3 ± 0.2	-1.3 ± 0.9

Figure 6. The tracked target location (red) on top of the ground truth position (black) is shown for the LR Dominant case with treatment interruption (grey) and applied couch shift. The mean $\pm$ standard deviation of the tracking error (ME) is also given.

Table 3. Treatment interruption test results. Presented are the mean $\pm$ standard deviation of the tracking error in each of the three motion directions.

Motion trace	Tracking error (mm)		
	LR	SI	AP
Sinusoidal	0.5 ± 0.2	0.1 ± 0.8	-0.4 ± 0.2
Baseline shift	1.3 ± 1.3	-0.2 ± 0.2	0.7 ± 1.1
Typical lung	0.5 ± 0.3	0.0 ± 0.6	-0.4 ± 0.4
High frequency	0.8 ± 0.4	0.0 ± 1.1	0.3 ± 0.8
LR dominant	1.2 ± 2.5	-0.3 ± 0.2	0.2 ± 0.8

Table 4. Dynamic localisation test results including the end-to-end latency.

Motion trace	Tracking error (mm)		
	LR	SI	AP
Sinusoidal	0.3 ± 0.9	-0.3 ± 3.1	-0.8 ± 0.4
Baseline shift	1.1 ± 1.7	-0.3 ± 0.3	-0.5 ± 1.0
Typical lung	0.6 ± 0.3	-0.1 ± 1.7	-0.5 ± 0.7
High frequency	0.7 ± 0.5	0.0 ± 3.0	-0.3 ± 0.6
LR dominant	1.0 ± 3.9	-0.3 ± 0.2	-1.3 ± 1.3

3.6. Test results taking end-to-end system latency into account

By the output time of markerless target tracking the target has changed its current position during the end-to-end system latency, which can additionally be included in the calculation of the tracking error. Taking the latency into account for the evaluation of the tracking results yields a mean $\pm$ standard deviation of the tracking error of 0.7 ± 1.9 mm (LR), -0.2 ± 2.0 mm (SI) and -0.7 ± 0.9 mm (AP) for the dynamic localisation tests. These values result in tracking margin components of 3.1 mm (LR), 1.9 mm (SI) and 2.4 mm (AP). Table 4 presents detailed results.

4. Discussion

Markerless lung target tracking was evaluated prospectively on a standard linear accelerator for the first time. Target position monitoring underwent multiple QA tests which included static and dynamic localisation accuracy and treatment interruption tests in a phantom experiment. The end-to-end system latency was also measured. All QA requirements were met successfully. An example for a markerless target tracking QA worksheet can be found in appendix. We suggest that the proposed QA tests should be repeated monthly as an addition to kV imaging system tests.

Markerless target tracking achieves its optimal accuracy for targets with predominantly SI motion e.g. in cases sinusoidal, typical lung and high frequency. Depending on the gantry angle, LR and AP motion occurs either perpendicular or parallel to the imaging direction. In the latter case, markerless target tracking relies on the implemented 3D inference, which is sensitive to tracking errors propagated from the template matching.

This leads to larger tracking errors when the target motion is pre-dominantly in the LR or AP direction e.g. for the motion traces baseline shift and LR dominant. In practice, the pre-treatment 4D-CT can be used to identify such motion characteristics and inform the reliability of markerless target tracking for each individual patient beforehand.

The 3D localisation can be used for various treatment adaptation strategies with or without accounting for the changes in depth. In a clinical implementation tracking margin components will be used to account for geometric uncertainties. For the determination of these margins the contribution of the mean tracking error is dominant (Van Herk 2004), leading the margins to be insensitive to occasionally occurring error peaks. Therefore, the tracking margin component for markerless target tracking is small compared to typical total margins in lung cancer radiotherapy (Benedict *et al* 2010).

Several aspects of markerless target tracking can be improved. The target localisation accuracy especially in SI-direction is limited by the quality and resolution of the planning 4D-CT which was used to build the model. Image artefacts due to motion blurring in 4D-CT can propagate to errors in the template matching step and affect the accuracy of markerless tracking. Further, it was found that additional objects in the 4D-CT, which differ between the CT scanner and the linac, such as the imaging couch and the treatment table, mislead the template matching approach. These can be removed from the model to improve localisation accuracy in the future. The localisation accuracy of markerless target tracking is inferior compared with marker-based tracking approaches (Santanam *et al* 2009, Kim *et al* 2017). However, the target is tracked directly avoiding surrogacy errors. The tracking margin components are likely subject to sampling errors as they are calculated from a small sample size of motion traces. They have yet to be verified for a large patient cohort. However, the results of the QA procedure can be considered as an estimate for the tracking accuracy needed to assist margin definition for patient treatments. Further, in the presented experimental setup the CIRS lung phantom was placed on the modified HexaMotion platform to enable 3D motion, however, this does not allow separate anatomy and target displacement. This setup was chosen based on the trade-off between the clinical feasibility of the setup complexity and the clinical relevance of the target tracking scenario. The conducted experiment was restricted by the geometric uncertainty of the modified HexaMotion platform and setup alignment (Cetnar *et al* 2016, Huang *et al* 2017).

Markerless target tracking delivers kV imaging dose that is similar to two CBCT acquisitions for each treatment fraction. Several strategies for dose reduction were identified and can be implemented in the future:

- The setup CBCT may replace the pre-treatment learning arc during the setup stage.
- The field of view of the kV imaging can be fitted to the motion range observed in the planning data for each patient individually.
- The imaging parameters can be optimised for the projection angle.
- Incorporating the imaging dose into the optimization framework can reduce the concomitant dose delivered (Grelewicz and Wiersma 2014).

The end-to-end latency of markerless target tracking was measured to 230 ms. It was found that the majority of this latency was caused by the frame streaming procedure (frame grabbing and writing image to disk) on top of the computational latency of 94 ms. Studies suggested that lung tumour motion prediction can compensate for system latencies (Sharp *et al* 2004, Krauss *et al* 2011) and a similar approach can be integrated in a future markerless target tracking implementation. Furthermore, the latency caused by the frame streaming procedure can potentially be significantly reduced from the future updates of the frame grabbing software (Lee *et al* 2018), or by directly passing the imaging data into the memory and bypassing the need to write data to the disk.

5. Conclusion

Markerless target tracking was implemented prospectively on a standard linear accelerator for the first time. Clinical process and QA practices for the safe clinical implementation have been developed and implemented for lung cancer VMAT. Markerless target tracking passed all QA tests. The QA procedure developed in this study paves the way for the clinical use of markerless target tracking on a standard linac.

Acknowledgments

Appendix. Markerless target tracking QA worksheet

Institution:	
Date:	
Physicist:	
Linac:	

Markerless QA Worksheet

The markerless QA phantom is placed on the motion stage and aligned with the linac's coordinate system by matching the lasers with the corresponding markers.

1. Place the motion stage on treatment table and initialise.
2. Place markerless QA phantom with 2cm tumour insertion on the stage.
3. Adjust the motion stage and treatment table to align the landmarks on the phantom with the lasers. Update origin of the motion stage.
4. Acquire setup CBCT and shift the tumour to the iso-centre.
5. Run the experiments.
6. The tracking margin component is calculated for the average tracking error in each direction according to:

$$M = 2.5 * ME + 0.7 * STD \qquad \text{(Van Herk formula)}$$

Static localisation

	Tracking error [mm]			Average tracking error [mm]			
Target shift	**LR**	**SI**	**AP**	**LR**	**SI**	**AP**	**Pass**
None							
LR + 5mm				**Tracking margin component [mm]**			
LR - 5mm				(<5mm required)			
SI + 5mm				**LR**	**SI**	**AP**	
SI - 5mm							
AP + 5mm							**YES**
AP - 5mm							**/NO**

Dynamic localisation

	Tracking error [mm]			Average tracking error [mm]			
Motion trace	**LR**	**SI**	**AP**	**LR**	**SI**	**AP**	**Pass**
Sinusoidal							
Typical Lung				**Tracking margin component [mm]**			
Baseline Shift				(<5mm required)			
LR Dominant				**LR**	**SI**	**AP**	**YES**
High Frequency							**/NO**

Treatment interruption (TI)

	Tracking error [mm]			Average tracking error [mm]			
Motion trace	**LR**	**SI**	**AP**	**LR**	**SI**	**AP**	**Pass**
Sinusoidal TI							
Typical Lung TI				**Tracking margin component [mm]**			
Baseline Shift TI				(<5mm required)			
LR Dominant TI				**LR**	**SI**	**AP**	**YES**
High Frequency TI							**/NO**

Latency

	Computation [ms]	**End-to-end [ms]**
Latency		

_____

Physicist signature

ORCID iDs

Marco Mueller ● https://orcid.org/0000-0002-3205-6979
Doan Nguyen ● https://orcid.org/0000-0003-1581-0359
Chun-Chien Shieh ● https://orcid.org/0000-0001-8245-8936

References

Adler J R Jr, Chang S D, Murphy M J, Doty J, Geis P and Hancock S L 1997 The cyberknife: a frameless robotic system for radiosurgery *Stereotactic Funct. Neurosurgery* **69** 124–8

Benedict S H *et al* 2010 Stereotactic body radiation therapy: the report of aapm task group 101 *Med. Phys.* **37** 4078–101

Booth J T, Caillet V, Hardcastle N, O'Brien R, Szymura K, Crasta C, Harris B, Haddad C, Eade T and Keall P J 2016 The first patient treatment of electromagnetic-guided real time adaptive radiotherapy using mlc tracking for lung sabr *Radiother. Oncol.* **121** 19–25

Bradski G 2000 The OpenCV Library *Dr. Dobb's Journal of Software Tools* **120** 122–5

Brandner E D, Chetty I J, Giaddui T G, Xiao Y and Huq M S 2017 Motion management strategies and technical issues associated with stereotactic body radiotherapy of thoracic and upper abdominal tumors: a review from nrg oncology *Med. Phys.* **44** 2595–612

Bryant J H, Rottmann J, Lewis J H, Mishra P, Keall P J and Berbeco R I 2014 Registration of clinical volumes to beams-eye-view images for real-time tracking *Med. Phys.* **41** 121703

Cerviño L I, Chao A K, Sandhu A and Jiang S B 2009 The diaphragm as an anatomic surrogate for lung tumor motion *Phys. Med. Biol.* **54** 3529

Cetnar A J, James J and Wang B 2016 Commissioning of a motion system to investigate dosimetric consequences due to variability of respiratory waveforms *J. Appl. Clin. Med. Phys.* **17** 283–92

Colvill E *et al* 2016 A dosimetric comparison of real-time adaptive and non-adaptive radiotherapy: a multi-institutional study encompassing robotic, gimbaled, multileaf collimator and couch tracking *Radiother. Oncol.* **119** 159–65

Fu D, Kahn R, Wang B, Wang H, Mu Z, Park J, Kuduvalli G and Maurer C R 2007 Xsight lung tracking system: a fiducial-less method for respiratory motion tracking *Treating Tumors that Move with Respiration* (Berlin: Springer) pp 265–82

Furtado H, Steiner E, Stock M, Georg D and Birkfellner W 2013 Real-time 2d/3d registration using kV-mV image pairs for tumor motion tracking in image guided radiotherapy *Acta Oncol.* **52** 1464–71

Gendrin C *et al* 2012 Monitoring tumor motion by real time 2d/3d registration during radiotherapy *Radiother. Oncol.* **102** 274–80

Glitzner M, Woodhead P L, Borman P T, Lagendijk J J and Raaymakers B W 2019 Mlc-tracking performance on the elekta unity MRI-linac *Phys. Med. Biol.* **64** 15NT02

Grelewicz Z and Wiersma R D 2014 Combined mV + kV inverse treatment planning for optimal kV dose incorporation in igrt *Phys. Med. Biol.* **59** 1607

Han X and Zhou Y 2019 Three dimensional localization and tracking for adaptive radiation therapy *US Patent Specification* 10/188,874

Hanley J *et al* 1999 Deep inspiration breath-hold technique for lung tumors: the potential value of target immobilization and reduced lung density in dose escalation *Int. J. Radiat. Oncol. Biol. Phys.* **45** 603–11

Haytmyradov M *et al* 2019 Markerless tumor tracking using fast-kV switching dual-energy fluoroscopy on a benchtop system *Med. Phys.* **46** 3235–44

Hazelaar C, Dahele M, Mostafavi H, van der Weide L, Slotman B and Verbakel W 2018 Markerless positional verification using template matching and triangulation of kV images acquired during irradiation for lung tumors treated in breath-hold *Phys. Med. Biol.* **63** 115005

Heinzerling J, Anderson J, Papiez L, Boike T, Chien S and Timmerman R 2007 Effectiveness of abdominal compression in stereotactic body radiation therapy (sbrt) treatment of lung and liver: 4d CT scan analysis of tumor and organ motion at varying levels of abdominal pressure *Int. J. Radiat. Oncol. Biol. Phys.* **69** S134–5

Hindley N, Keall P, Booth J and Shieh C C 2019 Real-time direct diaphragm tracking using kV imaging on a standard linear accelerator *Med. Phys.* **46** 4481–9

Hirai R, Sakata Y, Tanizawa A and Mori S 2019 Real-time tumor tracking using fluoroscopic imaging with deep neural network analysis *Phys. Med.* **59** 22–9

Hoisak J D and Pawlicki T 2018 The role of optical surface imaging systems in radiation therapy *Seminars in Radiation Oncology* **28** 185–93

Hsu A, Miller N, Evans P, Bamber J and Webb S 2005 Feasibility of using ultrasound for real-time tracking during radiotherapy *Med. Phys.* **32** 1500–12

Huang C Y, Keall P, Rice A, Colvill E, Ng J A and Booth J T 2017 Performance assessment of a programmable five degrees-of-freedom motion platform for quality assurance of motion management techniques in radiotherapy *Australas. Phys. Eng. Sci. Med.* **40** 643–9

Huang C Y, Tehrani J N, Ng J A, Booth J and Keall P 2015 Six degrees-of-freedom prostate and lung tumor motion measurements using kilovoltage intrafraction monitoring *Int. J. Radiat. Oncol. Biol. Phys.* **91** 368–75

Hugo G D, Liang J and Yan D 2010 Marker-free lung tumor trajectory estimation from a cone beam CT sinogram *Phys. Med. Biol.* **55** 2637

Kim J, Nguyen D, Huang C, Fuangrod T, Caillet V, O'brien R, Poulsen P, Booth J and Keall P 2017 Quantifying the accuracy and precision of a novel real-time 6 degree-of-freedom kilovoltage intrafraction monitoring (kim) target tracking system *Phys. Med. Biol.* **62** 5744

Krauss A, Nill S and Oelfke U 2011 The comparative performance of four respiratory motion predictors for real-time tumour tracking *Phys. Med. Biol.* **56** 5303

Lee D, Gholizadeh N, Wolf J, Nguyen D and Greer P 2018 Watchdog: a feasibility study to monitor respiratory motion for liver/lung cancer patients *Medical Physics* vol 45 (New York: Wiley) pp E275

Lewis J H, Li R, Watkins W T, Lawson J D, Segars W P, Cervino L I, Song W Y and Jiang S B 2010 Markerless lung tumor tracking and trajectory reconstruction using rotational cone-beam projections: a feasibility study *Phys. Med. Biol.* **55** 2505

Maurer C R Jr, West J and Jordan P 2015 Systems and methods for real-time tumor tracking during radiation treatment using ultrasound imaging *US Patent Specification* 9,108,048

Mori S *et al* 2016 Carbon-ion pencil beam scanning treatment with gated markerless tumor tracking: an analysis of positional accuracy *Int. J. Radiat. Oncol. Biol. Phys.* **95** 258–66

Ng J, Booth J, O'brien R, Colvill E, Huang C Y, Poulsen P R and Keall P 2014 Quality assurance for the clinical implementation of kilovoltage intrafraction monitoring for prostate cancer VMAT *Med. Phys.* **41** 111712

Poulsen P R, Cho B, Langen K, Kupelian P and Keall P J 2008 Three-dimensional prostate position estimation with a single x-ray imager utilizing the spatial probability density *Phys. Med. Biol.* **53** 4331

Rau A, Nill S, Eidens R and Oelfke U 2008 Synchronized tumour tracking with electromagnetic transponders and kV x-ray imaging: evaluation based on a thorax phantom *Phys. Med. Biol.* **53** 3789

Ren L, Zhang Y and Yin F F 2014 A limited-angle intrafraction verification (live) system for radiation therapy *Med. Phys.* **41** 020701

Richter A, Wilbert J, Baier K, Flentje M and Guckenberger M 2010 Feasibility study for markerless tracking of lung tumors in stereotactic body radiotherapy *Int. J. Radiat. Oncol. Biol. Phys.* **78** 618–27

Rottmann J, Keall P and Berbeco R 2013 Markerless epid image guided dynamic multi-leaf collimator tracking for lung tumors *Phys. Med. Biol.* **58** 4195

Rouabhi O, Gross B, Bayouth J and Xia J 2018 The dosimetric and temporal effects of respiratory-gated, high-dose-rate radiation therapy in patients with lung cancer *Technol. Cancer Res. Treat.* **18** 1533033818816072

Santanam L, Noel C, Willoughby T R, Esthappan J, Mutic S, Klein E E, Low D A and Parikh P J 2009 Quality assurance for clinical implementation of an electromagnetic tracking system *Med. Phys.* **36** 3477–86

Schmitt D, Nill S, Roeder F, Gompelmann D, Herth F and Oelfke U 2017 Motion monitoring during a course of lung radiotherapy with anchored electromagnetic transponders *Strahlentherapie Onkol.* **193** 840–7

Serpa M, Baier K, Cremers F, Guckenberger M and Meyer J 2014 Suitability of markerless epid tracking for tumor position verification in gated radiotherapy *Med. Phys.* **41** 031702

Shah A P, Kupelian P A, Waghorn B J, Willoughby T R, Rineer J M, Mañon R R, Vollenweider M A and Meeks S L 2013 Real-time tumor tracking in the lung using an electromagnetic tracking system *Int. J. Radiat. Oncol. Biol. Phys.* **86** 477–83

Sharp G C, Jiang S B, Shimizu S and Shirato H 2004 Prediction of respiratory tumour motion for real-time image-guided radiotherapy *Phys. Med. Biol.* **49** 425

Shieh C C, Caillet V, Dunbar M, Keall P J, Booth J T, Hardcastle N, Haddad C, Eade T and Feain I 2017 A bayesian approach for three-dimensional markerless tumor tracking using kV imaging during lung radiotherapy *Phys. Med. Biol.* **62** 3065

Shieh C C, Keall P J, Kuncic Z, Huang C Y and Feain I 2015 Markerless tumor tracking using short kilovoltage imaging arcs for lung image-guided radiotherapy *Phys. Med. Biol.* **60** 9437

Shimizu S, Shirato H, Ogura S, Akita-Dosaka H, Kitamura K, Nishioka T, Kagei K, Nishimura M and Miyasaka K 2001 Detection of lung tumor movement in real-time tumor-tracking radiotherapy *Int. J. Radiat. Oncol. Biol. Phys.* **51** 304–10

Suh Y, Dieterich S, Cho B and Keall P J 2008 An analysis of thoracic and abdominal tumour motion for stereotactic body radiotherapy patients *Phys. Med. Biol.* **53** 3623

Takao S, Miyamoto N, Matsuura T, Onimaru R, Katoh N, Inoue T, Sutherland K L, Suzuki R, Shirato H and Shimizu S 2016 Intrafractional baseline shift or drift of lung tumor motion during gated radiation therapy with a real-time tumor-tracking system *Int. J. Radiat. Oncol. Biol. Phys.* **94** 172–80

Teske H, Mercea P, Schwarz M, Nicolay N H, Sterzing F and Bendl R 2015 Real-time markerless lung tumor tracking in fluoroscopic video: handling overlapping of projected structures *Med. Phys.* **42** 2540–9

Van Herk M 2004 Errors and margins in radiotherapy *Seminars in Radiation Oncology* **14** 52–64

van Sörnsen de Koste J R, Dahele M, Mostafavi H, Sloutsky A, Senan S, Slotman B J and Verbakel W F 2015 Markerless tracking of small lung tumors for stereotactic radiotherapy *Med. Phys.* **42** 1640–52

Videtic G M, Hu C, Singh A K, Chang J Y, Parker W, Olivier K R, Schild S E, Komaki R, Urbanic J J and Choy H 2015 A randomized phase 2 study comparing 2 stereotactic body radiation therapy schedules for medically inoperable patients with stage i peripheral non-small cell lung cancer: Nrg oncology RTOG0915 (ncctg n0927) *Int. J. Radiat. Oncol. Biol. Phys.* **93** 757–64

Willoughby T, Lehmann J, Bencomo J A, Jani S K, Santanam L, Sethi A, Solberg T D, Tomé W A and Waldron T J 2012 Quality assurance for nonradiographic radiotherapy localization and positioning systems: report of task group 147 *Med. Phys.* **39** 1728–47

Wong J W, Sharpe M B, Jaffray D A, Kini V R, Robertson J M, Stromberg J S and Martinez A A 1999 The use of active breathing control (abc) to reduce margin for breathing motion *Int. J. Radiat. Oncol. Biol. Phys.* **44** 911–9

Yang Y, Zhong Z, Guo X, Wang J, Anderson J, Solberg T and Mao W 2012 A novel markerless technique to evaluate daily lung tumor motion based on conventional cone-beam CT projection data *Int. J. Radiat. Oncol. Biol. Phys.* **82** e749–56

Yin F F *et al* 2009 The role of in-room kV x-ray imaging for patient setup and target localization *Report of AAPM Task Group* 104

Zhang P, Hunt M, Telles A B, Pham H, Lovelock M, Yorke E, Li G, Happersett L, Rimner A and Mageras G 2018 Design and validation of a mV/kV imaging-based markerless tracking system for assessing real-time lung tumor motion *Med. Phys.* **45** 5555–63